Viscoelastic Changes in Os-Containing Poly(allylamine) Based Redox Hydrogels for Amperometric Enzyme Electrodes: An EQCM Study

E. J. Calvo*,† and R. Etchenique

INQUIMAE, Departamento de Química Inorgánica, Analítica y Química Física, Facultad de Ciencias Exactas y Naturales, Universidad de Buenos Aires, Pabellón 2, Ciudad Universitaria, AR-1428 Buenos Aires, Argentina

Received: June 7, 1999; In Final Form: August 6, 1999

Volume or mass and viscoelastic changes in $Os(byp)_2ClPyCH_2NH_2$−poly(allylamine) hydrogel (Os−PAA) cross-linked with glucose oxidase (GOx), have been measured by studying the electroacoustic impedance at 10 MHz. Film thickness and shear modulus have been obtained from imaginary and real components of the EQCM acoustic impedance in transient (cyclic voltammetry and chronoamperometry) as well as steady state oxidation and reduction of the hydrogel. Swelling of the film during Os^{II} oxidation resulted in mass uptake and decrease of shear modulus. These quantities depend only on the degree of polymer oxidation and not on film history or kinetics. Gravimetry beyond the Sauerbrey mass limit could be realized by use of Martin's viscoelastic model to treat the quartz crystal impedance.

Introduction

Chemically modified electrodes have attracted much attention of electrochemists over the last 15 years.[1−2] Modified electrodes have potential applications in electroanalysis, biosensors, electrocatalysis, energy conversion and storage, molecular devices and electrochromics, etc.[2] Redox conversion in polymer film modified electrodes is associated with the simultaneous exchange of ions and solvent with the bathing electrolyte in contact with the polymer. Thus, partition of solvent and ion transfer occur at the polymer−electrolyte interface during charge transfer at the electrode−polymer electrolyte and charge propagation in the polymer.

This gives rise to changes in mass due to exchange of ions and solvent and change in viscoelastic properties.[3] Changes in volume may result in variation of the distance between neighboring redox sites in redox and conducting polymers.

There has been a generalized impression that volume and viscoelastic changes occur simultaneously to redox switching as a consequence of solvent exchange. For a given polymer, these effects strongly depend on the nature of the solvent,[4] and for a particular solvent the ionic composition of the electrolyte may have a strong influence.[5]

The electrochemical quartz crystal microbalance (EQCM) has been extensively used to study polymer-modified electrodes, particularly as a gravimetric tool to follow the growth and redox switching processes.[3] However, for a linear frequency-to-mass relation to hold, the polymer overlayer must be rigid since otherwise viscoelastic changes also contribute to the frequency shift leading to an erroneous interpretation of the mass.[6]

The solvent incorporated into the polymer network leads to swelling and acts as a plasticizer of the polymer. Following the initial report of Buttry[7] who studied the viscoelastic changes in a polystyrene modified electrode with quartz crystal electroacoustic impedance, the measurement of the motional resistance R in addition to the resonant frequency of the quartz crystal was followed by numerous research groups.[8−13] However, most of these studies were qualitative and only discussed either the admittance spectral shape or reported the variation of the quartz crystal equivalent circuit parameters during electrochemical experiments.

Polymer behavior depends on the environment and oxidation state. For instance, a glassy polymer in air can become rubbery upon contact with the liquid electrolyte and subject to oxidation−reduction of the redox centers. Solvent population is dependent both on the electrolyte composition and film charge or redox state.

In the present communication we report volume and viscoelastic changes in a redox hydrogel (Os−PAA) by studying the electroacoustic impedance at 10 MHz of a quartz crystal covered by a thin Au electrode with the hydrogel film deposited onto the gold surface. The film thickness or mass and the shear modulus and their changes during oxidation and reduction have been obtained during oxidation−reduction of the redox layer using a viscoelastic model that considers the piezoelectric quartz covered by nonpiezoelectric viscoelastic layers.[14,15]

Experimental Section

Os−PAA hydrogel films were prepared on Au-coated quartz crystals by deposition of 3 μL of an aqueous solution consisting of 2 μL of 0.34% w/w Os−PAA of pH 6.0 in water with 2 μL 0.1% GOx in water and 2 μL of 2.2% PEDGE-400 (Polysciences), letting the solution gelate in water saturated air.[16]

Electrochemical Experiments. Gold-coated quartz crystals were employed. These crystals were 14 mm in diameter, 0.167 mm thick AT cut 10 MHz quartz crystals from International Crystal Manufacturing Company Inc. (Oklahoma City, OK, cat. 31210) with an active area of 0.196 cm^2.

A standard three-electrode electrochemical cell made of acrylic resin was used with an LM11 operational amplifier potentiostat with the working electrode (Au coated quartz) at real ground. This Au-coated quartz electrode was simultaneously

* Corresponding author.
† Permanent research staff of the Argentine Science Research Council (CONICET).

10.1021/jp991842r CCC: $18.00
Published on Web 10/04/1999

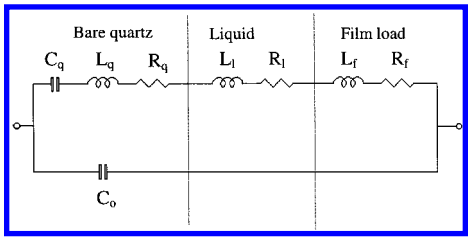

Figure 1. Modified Butterworth−Van Dyke equivalent electrical circuit for a quartz crystal resonator under mass, liquid, and viscoelastic film loading.

one of the quartz polarizing contacts at 10 MHz and the electrochemically working electrode. Two vinyl O-rings were used for sealing the quartz crystal with only one face of the crystal in contact with the electrolyte.

The reference electrode was a saturated calomel electrode (SCE) separated from the electrolyte by a fritted ceramic, and all potentials herein are quoted with respect to the SCE. A 1 cm^2 platinum mesh was used as the counter electrode.

Electroacoustic Measurement. The complex voltage divider to measure the resonant frequency and both components of the quartz crystal modified Butterworth−Van Dyke equivalent circuit has been described elsewhere.[17,18] In brief, a 10 MHz sinusoidal voltage (5 mV pp) generated by a voltage controlled oscillator (VCO) connected to the D/A output of a Keithley Data Acquisition System 575 was applied. Both the input V_i and output V_o voltage moduli were amplified (MAX436 rf op. amp) and rectified with an ideal diode circuit based on an LH0024 operational amplifier, and the resulting signals were measured with an A/D converter of the Keithley Data Acquisition System 575. An AT-386 computer generated the perturbation ac signal and calculated the ratio of circuit transfer function modulus, i.e., $|V_o/V_i|$ as a function of the VCO output signal frequency. The sample rate was 10 000 s^{-1}; thus, a complete transfer function spectrum (50 kHz and 100 points) was taken in 10 ms.

To correct for any shift of the VCO, the extreme frequencies were measured with a HP5334B frequency meter via an IEEE−488 interface. Calibration of the dc rectified signals was achieved with the read level functions of the HP5334B to the amplified rf signals used for frequency measurement.

The transfer function spectrum, modulus of V_o/V_i as a function of frequency around 10 MHz was obtained in real time for the quartz crystal in contact with the redox hydrogel and immersed in aqueous solution.

The modified lumped-element BVD electrical equivalent circuit is shown in Figure 1 and has been described elsewhere.[14] In brief, it consists of a static capacitance in parallel with a motional branch. The static capacitance C_0 is the result of two capacitances in parallel: the capacitance that arises between the electrodes located on opposite sides of the insulating quartz and the parasitic capacitance due to the cables and connections.[14] According to Martin,[14] the total capacitance of the motional arm C is considered to be equal to the capacitance of the quartz. The motional arm impedance is the sum of that due to the unperturbed or bare quartz with L_Q, R_Q, and C_Q; the liquid load with L_l and R_l; and the viscoelastic film load with L_f and R_f ($\mathbf{Z} = \mathbf{Z}_Q + \mathbf{Z}_l + \mathbf{Z}_f$). The motional arm lumped-elements R and L and the static capacitance, C_0, of the modified BVD equivalent circuit were obtained by nonlinear fit of the experimental transfer function spectrum data $|\mathbf{V}_o/\mathbf{V}_i|(\omega)$ to the analytical expression of the BVD transfer function:[18]

$$\left|\frac{\mathbf{V}_o}{\mathbf{V}_i}\right| = \frac{\sqrt{\left(\omega L - \frac{1}{\omega C}\right)^2 + R^2}}{\sqrt{\left(\omega L - \frac{1}{\omega C} + \frac{\omega L C_0}{C_m} - \frac{C_0}{\omega C C_m} - \frac{1}{\omega C_m}\right)^2 + \left(R + \frac{R C_0}{C_m}\right)^2}} \quad (1)$$

where C_m is the measuring capacitance in series with the BVD,-with $j = \sqrt{-1}$, $\omega = 2\pi f_s$, and f_s is the resonant frequency.

Quartz Crystal Impedance

For a system of nonpiezoelectric layers attached to the quartz resonator, Granstaff and Martin[15] derived an expression for the total electrical equivalent impedance $\mathbf{Z}$ in terms of the surface mechanical impedance $\mathbf{Z}_M$.

$$Z = \frac{2\omega L_Q}{\pi\sqrt{\mu_Q \rho_Q}} Z_M = R + jX_L \quad (2)$$

with $X_L = \omega L$, $L_Q \approx 7.5$ mH for 10 MHz AT-cut quartz crystals and $\mu_Q = 2.957 \times 10^{10}$ N m^{-2} is the elastic constant for piezoelectrically stiffened quartz, and $\rho_Q = 2650$ kg m^{-3} is the density of the quartz.

The mechanical impedance of each nonpiezoelectric layer on the quartz is given by[15]

$$\mathbf{Z}_M = \sqrt{\rho \mathbf{G}} \tanh(\mathbf{k}d) \quad (3)$$

where $\mathbf{G} = G' + \mathbf{j}G''$ is the complex shear modulus of the nonpiezoelectric layer at 10 MHz, $\mathbf{k} = \mathbf{j}\omega\sqrt{\rho/\mathbf{G}}$, the wave propagation constant d is the thickness of the nonpiezoelectric layer of density ρ.

If the layer is thick enough ($d \rightarrow \infty$), the shear wave vanishes in the bulk of the layer and no energy is transferred from this point. In this case, $\tanh(\mathbf{k}d) \rightarrow 1$ and $\mathbf{Z}_M = \mathbf{Z}_M^* = \sqrt{\rho \mathbf{G}}$, where the superscript * indicates the semi-infinite approximation.

For small changes in X_{LM}, corresponding to a small deposited mass, the variation in resonant frequency can be approximated as linear on X_{LM} and the Sauerbrey equation holds:[19]

$$\Delta f_0 \cong \frac{-2 f_0^{\,2}}{\sqrt{\mu_Q \rho_Q}} \frac{\Delta m}{A} \quad (4)$$

where A is the active area of the piezoelectric resonator and Δm is the variation in the electrode mass (Sauerbrey mass).

If two nonpiezoelectric layers are successively attached to the crystal, the following expression describes the surface impedance:[15]

$$\mathbf{Z}_S = \frac{2\omega L_Q}{\pi\sqrt{\mu_Q \rho_Q}} \left(\frac{\mathbf{Z}_f^* \tanh(\mathbf{k}_f d_f) + \mathbf{Z}_l^* \tanh(\mathbf{k}_l d_l)}{1 + \frac{\mathbf{Z}_l^*}{\mathbf{Z}_f^*} \tanh(\mathbf{k}_f d_f) \tanh(\mathbf{k}_l d_l)} \right) \quad (5)$$

where the subscript f denotes the viscoelastic film underlayer and the subscript l the liquid overlayer, respectively.

If the mechanical interaction between both layers is negligible, the denominator tends to unity and additivity of the layer impedances holds; that is,

$$\mathbf{Z} = \frac{2\omega L_Q}{\pi\sqrt{\mu_Q \rho_Q}}(\mathbf{Z}_f^* \tanh(\mathbf{k}_f d_f) + \mathbf{Z}_l^* \tanh(\mathbf{k}_l d_l)) \quad (6)$$

In the case of two layers with comparable mechanical impedances, the interaction between both layers cannot be neglected and the full eq 5 should be used. We can describe the contribution of the viscoelastic layer to the total quartz crystal impedance Z at 10 MHz in terms of film properties,[15]

$$Z_f = R_f + j\omega L_f = \frac{2\omega L_Q}{\pi\sqrt{\mu_Q \rho_Q}}\left(\sqrt{\rho_f G_f}\tanh\left(j\omega d_f \sqrt{\frac{\rho_f}{G_f}}\right)\right) \quad (7)$$

where d_f is the polymer film thickness, ρ_f its density, and $\mathbf{G}_f$ the viscoelastic complex shear modulus ($G'_f + jG''_f$) with $\mathbf{G}'_f$ the storage modulus and $\mathbf{G}''_f$ the loss modulus of the viscoelastic film at 10 MHz.

When additivity holds and eq 6 can be used, the motional impedance for the modified BVD equivalent circuit is given by the sum of the unperturbed resonator $\mathbf{Z}_Q = \mathbf{R}_Q + j\mathbf{X}_{LQ}$, the liquid load $\mathbf{Z}_l = \mathbf{R}_l + j\mathbf{X}_{Ll}$, and the viscoelastic film load $\mathbf{Z}_f = R_f + j\mathbf{X}_{Lf}$ which contribute to the mechanical impedance of the composite resonator, $\mathbf{Z} = \mathbf{Z}_Q + \mathbf{Z}_l + \mathbf{Z}_f$.

The lumped-element model (LEM) model assumes that the surface load impedance is negligible as compared to the surface mechanical impedance of the quartz and that the resonator operates near mechanical resonance.[17] The validity of the LEM equivalent circuit to within 1% of the transmission line model[17] is fulfilled since the ratio of the surface film and/or liquid impedance ($\mathbf{Z}_s$) to the quartz impedance ($\mathbf{Z}_q$) is $\mathbf{Z}_s/\mathbf{Z}_q < 0.005$.

Use of eq 6 also assumes additivity of the surface film ($\mathbf{Z}_f$) and liquid electrolyte ($\mathbf{Z}_l$) mechanical impedances in eq 5 which is valid for $|Z_f| \gg |Z_l|$ or for very thin films ($d_f \rightarrow 0$).[15] For aqueous electrolytes $|Z_l| \approx 280\ \Omega$ and $G = j\omega\eta$, where η is the viscosity of water and the film impedance Z_f at 10 MHz can be obtained by subtracting the impedance due to the Newtonian liquid electrolyte (ca. $X_{Lf} \approx R_f$) from the surface impedance Z_S due to film and liquid.

Results and Discussion

Figure 2 shows the simultaneous cyclic voltammogram at 10 mV s^{-1} (a) and the film electroacoustic impedance components R_f (b) and X_{Lf} (c) in the vicinity of the resonance frequency $f_s \approx 10$ MHz for an Au-coated quartz crystal loaded with a thick layer of Os−PAA−GOx hydrogel layer (approximately 1.7 μm) and immersed in 0.1 M $NaNO_3$ and 50 mM TRIS buffer of pH 7.2 aqueous electrolyte.

The typical cyclic voltammogram of the Os film coated electrode shown in Figure 2a has been described elsewhere.[16] The main features of Os−PAA hydrogel are high stability, unlike previously studied ferrocene-modified PAA gels, with diffusional behavior, i.e., the film is never completely oxidized nor fully reduced in the time scale of the experiment as can be seen in Figure 2a. The surface confined Os^{III}/Os^{II} redox couple shows a reversible cyclic voltammogram with 56 mV peak separation and typical diffusional tailing with linear dependence of the peak current with the square root of the potential sweep rate. The quantity $cD^{1/2}$ evaluated with the Sevick−Randles eq 20 gives typical values in the range $(3-4) \times 10^{-9}$ mol cm^{-2} $s^{-1/2}$.

A linear negative shift of the Os^{III}/Os^{II} redox potential in the poly(allylamine) film with the logarithm of the KNO_3 concentration gives evidence of Donnan perm selectivity with anion exchange.[10,21] Since anions can move rapidly in the highly hydrated gel, the diffusion-like propagation of charge in these films has been attributed to electron hopping between adjacent Os sites. Simultaneous drag of solvent as the ions ingress into the swollen polymer matrix results in swelling of the film as will be shown below.

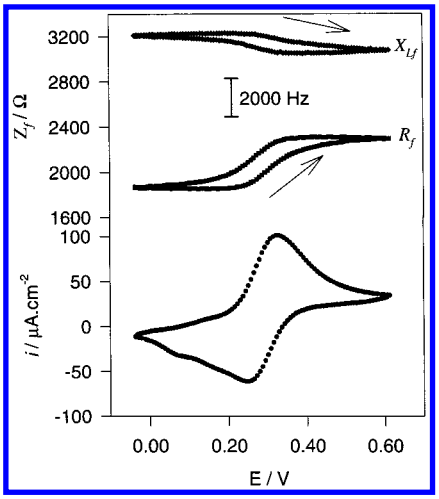

Figure 2. Current−potential curve during cyclic voltammetry of Os−PAA−Gox hydrogel modified electrode in 50 mM Tris buffer of pH 7.2 and 0.1 M KNO_3 supporting electrolyte at 0.01 V s^{-1} (a) and simultaneous R_f (b) and X_{Lf} (c).

In Figure 2b, R_f increases continuously during the oxidation of the reduced Os^{II} gel, while in Figure 2c, X_{Lf} decreases as the film is oxidized; the opposite trend is observed upon film electroreduction. A classical interpretation of a positive resonant frequency shift based on the Sauerbrey equation (eq 4) would indicate that the mass decreases. However, the high damping resistance R_f indicates that the acoustic wave is highly attenuated in the Os−PAA gel which behaves as a viscoelastic nonrigid layer at 10 MHz and therefore the Sauerbrey equation cannot be used since an important viscoelastic/volume change occurs.

The Os−PAA modified electrodes were also studied by chronoamperometry where the electrode potential is fixed and the current time course accounts for the redox concentration relaxation. Typical oxidation and reduction current transients for potential steps between the extreme potentials in Figure 2a are shown in Figures 3d and 4c, from which values of $C_T D_e^{1/2}$ were obtained with the Cottrel equation[20] in agreement with those obtained by cyclic voltammetry. Independent measurement of the apparent total redox concentration C_T and electron diffusion coefficient D_e were obtained by chronoamperometry at ultramicroelectrodes (UME) and analysis of the current transient with the Soup−Szabo equation as described elsewhere.[22] Values of $C_T \approx 0.3-1$ M and $D_e \approx 10^{-9}$ to 10^{-10} cm^{-2} s^{-1} were obtained for these films.

The film electroacoustic impedance components R_f and X_{Lf} evolution with time simultaneous to the oxidation and reduction current are shown in Figures 3a,b and 4a,b and follow the same trend as in the cyclic voltammetry; X_{Lf} decreases and R_f increases for Os−PAA film oxidation, while the opposite is apparent during the reduction step. Recovery of the initial values demostrates the reversibility of the process.

When excess glucose is present in the electrolyte instead of the cyclic voltammetry shown in Figure 2a, a steady-state catalytic wave is observed with a half wave potential that coincides with the redox potential of the Os^{II}/Os^{III} redox couple in the film.[16] The steady-state catalytic current in Figure 5 arises from the enzymatic oxidation of glucose catalyzed by GOx in the gel and mediated by the Os−PAA polymer according to

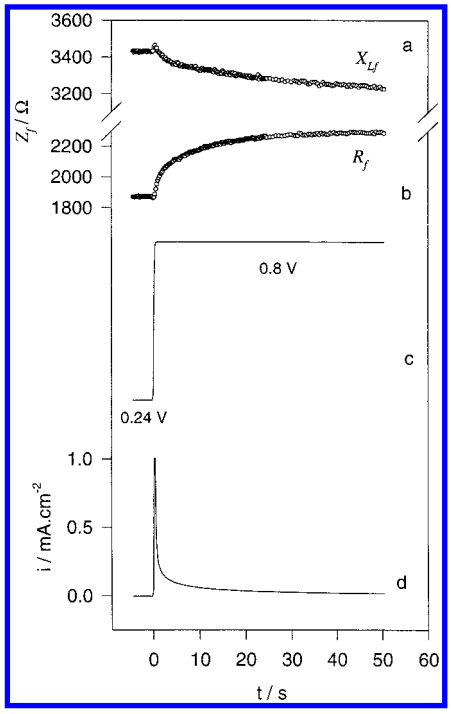

Figure 3. Chronoamperometry of an Os−PAA−GOx modified electrode for the oxidation $Os^{II} \rightarrow Os^{III}$ (d) from 0 to 0.5 V (c) and simultaneous 10 MHz quartz crystal impedance components X_{Lf} (a) and R_f (b).

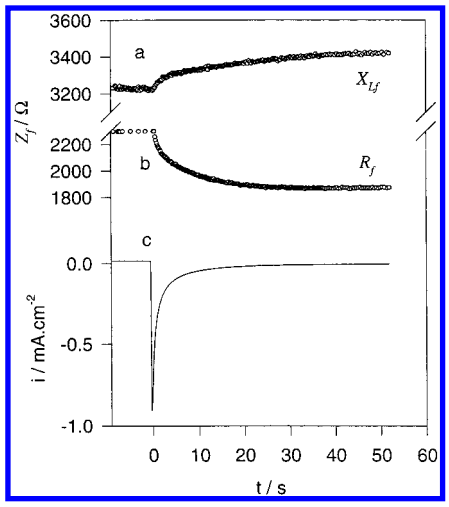

Figure 4. Reverse chronoamperometry of the Os−PAA−Gox modified electrode of Figure 4 during a potential step from 0.5 to 0 V for the reduction of Os^{III} (c) and simultaneous 10 MHz quartz crystal impedance components due to the surface film (a,b).

the following reaction scheme:[23]

$$\beta\text{-D-glucose} + \text{GOx(FAD)} \rightarrow \text{gluconic acid} + \text{GOx(FADH}_2\text{)} \quad (8)$$

$$\text{GOx(FADH}_2\text{)} + 2\text{Os}^{III} - \text{PAA} \rightarrow \text{GOx(FAD)} + 2\text{Os}^{II} - \text{PAA} + 2\text{H}^+ \quad (9)$$

with regeneration of Os^{III}−PAA at the underlying Au electrode and charge propagation by electron hopping in the polymer gel by a diffusion-like process arising from electron hopping between neighboring redox sites at appropriate tunneling distance.

During the enzyme redox double catalytic cycle described by eqs 8 and 9, the interplay of electron diffusion between redox adjacent sites and enzyme catalysis sets a steady-state concentration gradient of Os^{III} from the underlying Au electrode to the external electrolyte.

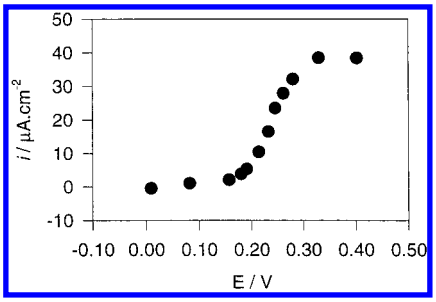

Figure 5. Steady state catalytic current for the oxidation of 0.1 M glucose in 50 mM Tris buffer of pH 7.2 and 0.1 M KNO_3.

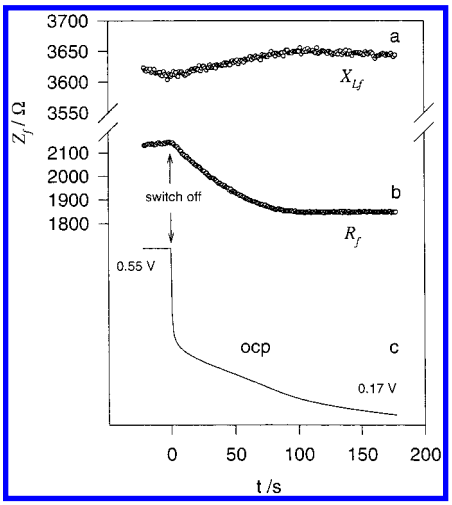

Figure 6. Enzymatic reduction of Os^{III}−PAA−GOx by glucose during a switch off experiment from the oxidized Os^{III} state and open circuit potential evolution (c) and simultaneous evolution of the film electroacoustic impedance parameters (a,b).

The viscoelastic/volume properties responsible for the electroacoustic film impedance (X_{Lf} and R_f) are dependent on the redox composition as will be shown below and the redox concentration profile changes across the film. Therefore, for steady state enzyme-redox catalysis, there is an inhomogeneous distribution of redox states in the direction perpendicular to the electrode surface. Then, as it will be justified below, the electroacoustic impedance results from spatially averaged properties such as film density, viscoelastic modulus, and thickness that vary with distance from the Au electrode and with the electrode potential.

The Os^{III} polymer can also be reduced chemically in the presence of glucose in solution after polarization at 0.5 V for 2 min by switching off the electrode. Under open circuit conditions, glucose can reduce GOx(FAD) which subsequently reduces the Os^{III} sites in the Os−PAA film as shown by the evolution of the open circuit potential (ocp) that reaches a value corresponding to the totally reduced state (0.17 V in Figure 6c).

After current interruption, the quartz impedance parameters were followed as a function of time and the resulting transients are shown in parts a and b of Figure 6. In a similar current interruption experiment but in the absence of glucose in solution in contact with the gel, the electrode potential shows memory as can be followed by the ocp which remains close to the polarizing potential prior to switch off (in the oxidized state).

In the presence of enzyme substrate, glucose in solution reduces those Os^{III} centers in the hydrogel that "wire" or connect the enzyme GOx to the underlying gold electrode. Therefore,

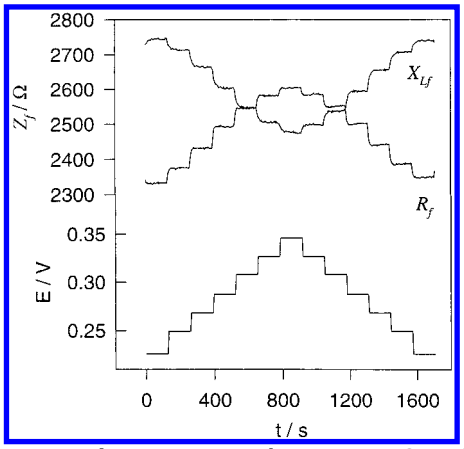

Figure 7. Potential staircarse perturbation to an Os−PAA−GOx hydrogel modified electrode and values of the 10 MHz film electroacoustic impedance as a function of time for the oxidation and reduction of the film. From 0.225 V (totally reduced film) in 20 mV steps.

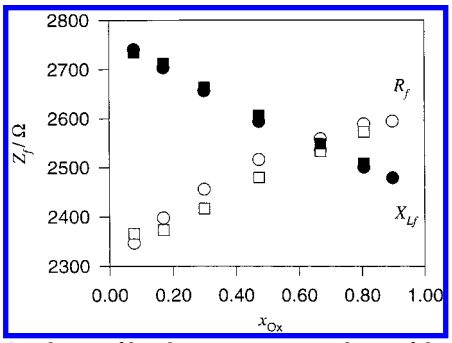

Figure 8. Steady state film electroacoustic impedance of the Os surface film as a function of the fraction of Os^{III} concentration calculated from Figure 7 and using the Nernst equation. With $E^{\circ\prime} \approx E_{1/2}$.

from parts a and b of Figure 6 it can be seen that enzymatic reduction of the hydrogel by glucose also results in transient changes of X_{Lf} and R_f in the same direction as electrochemical reduction in Figure 4 since the steady state concentration that corresponds to the initial anodic polarization relaxes yielding a totally reduced Os^{II}−PAA film with conversion of glucose into gluconic acid.

The evidence presented so far for transient experiments has established that R_f and X_{Lf} vary with Os film oxidation and reduction either chemically or electrochemically and that full recovery of the initial state was obtained.

To distinguish if there is a dependence on the polymer redox state or if kinetic effects are responsible for the transient response, a potential staircase perturbation was applied to the Os film from the reduced to the oxidized state and backward to the Os^{II} state. The time length of each potential step was long enough to reach a homogeneous redox concentration within the film as indicated by the current transients reaching zero current (not shown).

The potential staircase perturbation and the resulting values of R_f and X_{Lf} are depicted in Figure 7 in both forward and backward directions. It can be seen in Figure 7 that stationary film impedance was attained at each potential.

The steady-state values of Z_f are shown in Figure 8 as a function of the Os^{III} fraction ($x_{Os(III)}$) in the film. It should be noted that there is no hysteresis between oxidation and reduction directions and therefore R_f and X_{Lf} are solely dependent on the state of film oxidation. Thus, the transient results are indicative of concentration relaxation within the film and not of kinetic effects. Also, in Figure 8 a nearly linear dependence of both impedance components with the fraction of Os^{III} is apparent.

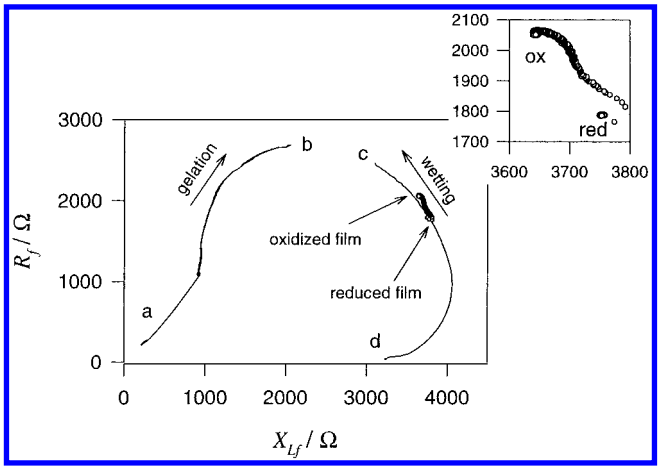

Figure 9. Parametric plots of the real to imaginary components of the 10 MHz film electroacoustic impedance for the formation by sol−gel transformation, dehydration, and redox switching of the Os−PAA−Gox hydrogel. a → b sol−gel; c → d dehydration and redox switching (inset).

We have introduced parametric quartz crystal impedance plots, R_f vs X_{Lf}, to analyze the effect of mass or volume and viscoelastic changes of the film in contact with the electrolyte overlayer while the film undergoes changes in its redox state.[18] Figure 9 depicts such a parametric plot of R_f as a function of X_{Lf} following the history of the film along the parametric curve as the hydrogel is formed by sol−gel transformation (a → b) from an infinite liquid (linear portion on the low left corner in Figure 9) by increasing viscosity and by water evaporation into a finite gel layer (c to d portion) with time as the variable parameter for both components of the film impedance at 10 MHz.

As will be explained below, from curve fitting using eq 7, in the region near the electrochemical experiment, the loss tangent ($\alpha = G''/G'$) was evaluated, and it resulted as $\alpha \approx 2.5$ for this film.

Sol−gel formation of the film and drying moves the film impedance through the parametric curve from left to right. Oxidation−reduction of the Os−PAA film, on the other hand, moves the film impedance in a small sector (see inset Figure 9) of the parametric plot with simultaneous change in film thickness and shear modulus.

Note that the small displacement on the parametric plot during oxidation−reduction of the Os^{II}/Os^{III} couple in the film takes place in a region that is far from the Sauerbrey limit that corresponds to rigid mass ($R_f = 0$).

By defining two parameters in eq 7 such as the film density ρ_f and the loss tangent $\alpha = G''/G'$, we can obtain the evolution of the film thickness d_f and shear modulus $|\mathbf{G}| = (\mathbf{G}'^2 + \mathbf{G}''^2)^{1/2}$ as a function of time or electrode potential. In the present case, we have assumed that $\rho_f \approx 1000$ kg m^{-3} since PAA−Os is a hydrogel with high water content due to the large amount of ionizable NH_2 groups; therefore, incorporation of solvent and ions is not likely to change ρ_f appreciably. The experimental values of R_f and X_{Lf} at different time or potential were used to solve eq 7 for $|\mathbf{G}|$ and d_f using a two-dimensional root-finding algorithm (secant method) and $\rho_f = 1000$ kg m^{-3} and $\alpha = 2.5$ with error of <0.01 Ω for R_f and X_{Lf}.[17]

The initial impedance components for the dry film are $X_{Lf} \approx 3.250$ Ω and $R_f \approx 0$. Under those conditions, the Sauerbrey approximation holds and the resulting film thickness is 1.5 μm. After saturation in a wet atmosphere ($a_{H_2O} = 1$), R_f increases continuously during water uptake and reaches 2.500 Ω, which

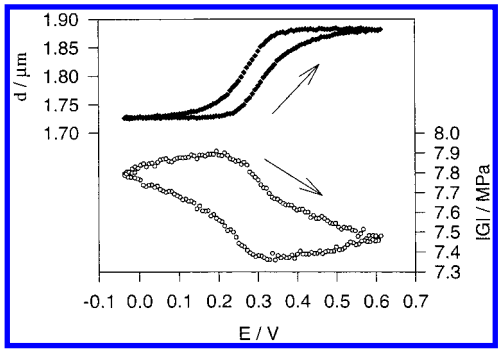

Figure 10. Plot of d_f and $|\mathbf{G}|$ as a function of electrode potential for data in Figure 2

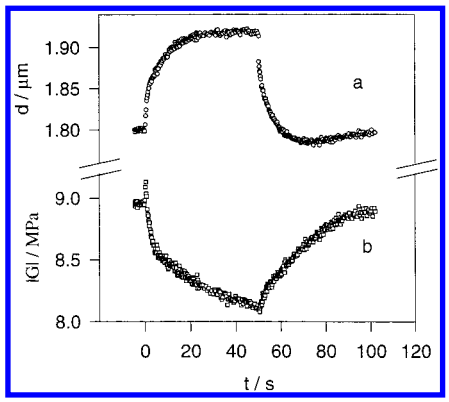

Figure 11. Plot of d_f (a) and $|\mathbf{G}|$ (b) calculated with eq 7 for the oxidation and reduction of Os^{II}/Os^{III} redox film for data in Figures 3 and 4.

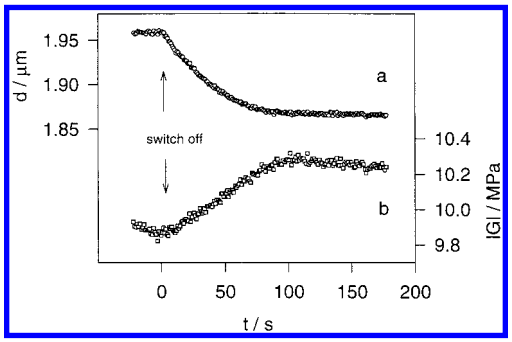

Figure 12. Plot of d_f (a) and $|\mathbf{G}|$ (b) calculated with eq 7 for a switch-off experiment after potentiostating the hydrogel enzyme electrode at 0.55 V in 50 mM glucose solution (Figure 6).

indicates a strong viscoelastic behavior of the hydrated film.[24] The thickness (mass) increases by 0.50 μm (30%) while $|\mathbf{G}|$ decreases from $(2-3) \times 10^8$ Pa to less than 10^7 Pa.

While the dry film behaves at 10 MHz as a glassy polymer, as suggested by the value of $|\mathbf{G}|$,[25] it becomes rubbery after hydration; therefore, the rigid mass approximation used for the dry film is no longer valid for the hydrated polymer. Under hydration, the dry glassy polymer undergoes a process similar to glass to rubbery polymer transformation as water is incorporated into the gel decreasing the electrostatic attraction between polycationic Os−PAA and polyanionic glucose oxidase.

The variation in d_f and $|\mathbf{G}|$ calculated by fitting the experimental film electroacoustic impedance data with eq 7 is shown in Figures 10, 11, and 12 for cyclic voltammetry, chronoamperometry, and switch off experiments, respectively, that correspond to the film impedance components shown in Figures 2−4 and 6. Note that while X_{Lf} decreases (Δf increases) and R_f increases upon film oxidation there is an increase of film thickness. The Sauerbrey equation (eq 4) would have predicted a mass decrease for an increase in resonant frequency. However, since the film acoustic impedance in the polar plot of Figure 9 (inset) is in a region far from the rigid mass, an increase in mass, simultaneous to a decrease in $|\mathbf{G}|$, results in a decrease of X_{Lf} and an increase of R_f.

In the polar plot shown in Figure 9, the increase of the viscoelastic shear modulus at constant thickness corresponds to a clockwise displacement on the parametric curves while an increase in thickness at constant density (mass) moves the impedance to an outer curve.

Therefore, as we have shown in a recent communication,[26] it is possible to make gravimetric measurements beyond the Sauerbrey approximation provided Martin's viscoelastic model is used to interpret the changes in electroacoustic impedance elements.

In chronoamperometric experiments, the same trend as seen in the cyclic voltammetry is apparent in Figure 11 with thickness increase and the shear modulus decrease with oxidation. Recovery of the initial state of these variables is also apparent.

Note that swelling and shrinking phenomena in these hydrogels occur on the same time scale. This is thought to be due to the high water content in the hydrogel. For polymer films in which one of the states is highly solvated while the other redox state is less solvated, the ingress and egress of ions occurs with different time constants.[5]

Reduction of the film by the enzymatic oxidation of glucose at open circuit also results in a decrease of d_f with an increase of the shear modulus at open circuit as shown in Figure 12 in analogy to the electrochemical reduction of the Os film shown in Figure 11.

Analysis of a linear plot of film mass ($\rho_f d_f A$) versus electrical charge for the oxidation of Os−PAA film has yielded 2.45 mg $coul^{-1}$ or 236 g per equivalent of Os^{III} formed. Since this value is much larger than the molar mass of any ion present in solution, we conclude that most of the mass increase (decrease) during oxidation (reduction) arises from solvent incorporation into the film. Thus, the large uptake of water must be related to polymer dynamics as Os^{II} sites are oxidized and to the hydrophillicity of the polymer due to the large amount of NH_2 groups in the film.

While for non-steady-state techniques a redox concentration gradient across the film is set up by the current flow, under conditions of zero current a homogeneous redox concentration across the film is expected. So, in transient experiments, the value of the shear modulus obtained is spatially averaged because a redox concentration gradient is established across the film at each time while steady-state experiments yield an homogeneous and concentration-dependent shear modulus.

The steady-state values of thickness and shear modulus are depicted in Figure 13 as a function of the degree of polymer film oxidation (x_{Ox}). It can be seen that the thickness and shear modulus are clearly dependent on the degree of oxidation with nearly linear increase of the film thickness with Os^{III} redox concentration and negligible hysteresis for the oxidation or reduction direction. The decrease of shear modulus with Os^{III} in the film, on the other hand, is not linear leveling above halfway oxidation.

In our previous report,[17] two limiting cases were analyzed for similar ferrocene−poly(allylamine) hydrogel layers of the same composition but different thickness. For acoustically thin films at 10 MHz, the Sauerbrey approximation was valid and changes of mass or thickness and film viscosity that resulted from the anion and water exchange were measured during redox

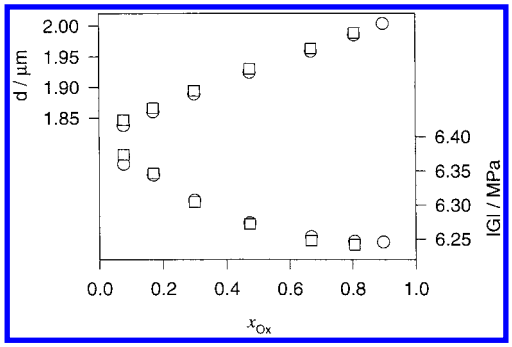

Figure 13. Dependence of the values of d_f and $|\mathbf{G}|$ calculated from R_f and X_{Lf} in Figure 7 with eq 7 as a function of the degree of Os film oxidation.

conversion. For acoustically thick gels at 10 MHz, on the other hand, the penetration depth of the acoustic shear wave resulted far less than the film thickness ($d_f \gg \lambda = (\eta/\omega\rho_f)^{1/2}$) and a liquidlike behavior was apparent. In that case, the film storage modulus (G') and the shear loss modulus ($G'' = \omega\eta$) were evaluated simultaneously to the redox conversion from the measured R_f and X_{Lf} ($=\omega L_f$) values with the EQCM.

The values of $|\mathbf{G}|$ in the Mpa range found in the present work for Os−PAA film are comparable to those reported for the Fc−PAA hydrogel.[17] Studies with the EQCM at different electrolyte ionic strength have also shown that the shear modulus in polycationic poly(allylamine) hydrogels cross-linked with negatively charged glucose oxidase (GOx) arises from electrostatic interactions.[17,18]

At 10 MHz, the relaxation of the ionic atmosphere of the polyelectrolyte dominates the ultrasound absorption[27] and therefore the shear modulus describes the elastic energy stored in ionic pairing and the viscous damping due to the friction of the poly(allylamine) chains in a gel swollen by solvent and electrolyte.

The shear modulus at 10 MHz $|\mathbf{G}|$ decreases with the degree of Os^{II} oxidation (Figure 13) by 2% from the fully reduced to the fully oxidized redox polymer, which is consistent with our previous finding in similar hydrogels of a strong potential-dependent decrease in G'' with oxidation in these films.

These results are relevant for polymer microgravimetry since it is generally recognized the difficulty to obtain the exact contribution of ionic exchange because ion transport is usually accompanied by solvent transport.[28]

Furthermore, swelling may lead to changes in the average site-to-site distance between neighboring redox centers and the variation of shear modulus would reflect the viscosity of the hydrogel at 10 MHz. Although small, these changes are expected to influence the apparent electron diffusion coefficients depending on the redox state of the gels, and further studies are in progress in order to verify current ideas on the dynamics of electron hopping.[29,30]

Conclusions

Viscoelastic and volume changes during redox switching of Os−PAA hydrogel both in transient (cyclic voltammetry and chronoamperometry) and steady-state oxidation−reduction of the Os sites have been measured with the EQCM using electroacoustic impedance.

Variation of the film thickness due to swelling of the hydrogel upon oxidation was measured in real time outside the Sauerbrey limit based on Martin's viscoelastic model.

The values of d_f (film thickness) and $|\mathbf{G}|$ (shear modulus) only depend on the oxidation state of the hydrogel and not on the film history or kinetics.

Acknowledgment. The authors acknowledge The Argentine Science Research Council (CONICET, Grant PICT-0054), The National Agency for Science and Technology Promotion (ANPCyT, Grant 06-00151-02434), The University of Buenos Aires (Grant Ubacyt-TW76), and Fundacion Antorchas for financial support.

References and Notes

(1) Murray, R. W. In *Molecular Design of Electrode Surfaces*; Murray, R. W., Ed.; John Wiley & Sons Inc.: New York, 1992; Chapter 1, p 1.
(2) Murray, R. W. In *Electroanalytical Chemistry*; Bard, A. J., Ed.; Marcel Dekker: New York, 1984; Vol. 13, p 192.
(3) Buttry, D. A.; Ward, M. D. *Chem. Rev.* **1992**, *92*, 1355.
(4) Oyama, N.; Ohsaka, T. *Prog. Polym. Sci.* **1995**, *20*, 761.
(5) Kelly, D. M.; Vos, J. G.; Hillman, A. R. *J. Chem. Soc., Faraday Trans.* **1996**, *92*, 4101.
(6) Topart, P. A.; Noel, M. A. M. *Anal. Chem.* **1994**, *66*, 2926.
(7) Borjas, R.; Buttry, D. A. *J. Electroanal. Chem.*. **1990**, *280*, 73.
(8) Muramatsu, H.; Ye, X.; Suda, M.; Sakuhara, T.; Ataka, T. *J. Electroanal. Chem.* **1992**, *322*, 311.
(9) Muramatsu, H.; Ye, X.; Ataka, T. *J. Electroanal. Chem* **1883**, *347*, 247.
(10) Oyama, N.; Tatsuma, T.; Takahashi, K. *J. Phys. Chem* **1993**, *97*, 10504.
(11) Ikeda, S.; Oyama, N. *Anal. Chem.* **1993**, *65*, 1910.
(12) Skompska, M.; Hillman, A. R. *J. Chem. Soc., Faraday Trans.* **1996**, *92*, 4101.
(13) Clarke, A. P.; Vos, J. G.; Glidle, A.; Hillman, A. R. *J. Chem. Soc., Faraday Trans.* **1993**, *89*, 1695.
(14) Martin, S. J.; Granstaff, V. E.; Frye, G. C. *Anal. Chem.* **1991**, *63*, 2272.
(15) Granstaff, V. E.; Martin, S. J. *J. Appl. Phys.* **1994**, *75*, 1319.
(16) Danilowicz, C.; Corton, E.; Battaglini, F.; Calvo, E. J. *Electrochim. Acta* **1998**, *43*, 3225.
(17) Etchenique, R. A.; Calvo, E. J. *Anal. Chem.* **1997**, *64*, 4833.
(18) Calvo, E. J.; Etchenique, R.; Bartlett, P. N.; Singhal, K.; Santamaria, C. *Faraday Discuss.* **1997**, *107*, 141.
(19) Sauerbrey, G. *Z. Phys.* **1959**, *155*, 206.
(20) Bard, A. J.; Faulkner, L. R. *Electrochemical Methods: Fundamentals and Applications*; John Wiley: New York, 1980.
(21) Doblhofer, K.; Vorotynstev, M. In *Electroactive Polymer Electrochemistry. Part 1. Fundamentals*; Lyons, M. E. G., Ed.; Plenum Press: New York, 1994; Chapter 3.
(22) Battaglini, F.; Calvo, E. J.; Danilowicz, C.; Wolosiuk, A. *Anal. Chem.* **1999**, *71*, 1062.
(23) Calvo, E. J.; Etchenique, R.; Danilowicz, C.; Diaz, L. *Analytical Chemistry* **1996**, *68*, 4186.
(24) Etchenique, R.; Calvo, E. J. In preparation.
(25) Ferry, J. D. *Viscoelastic Properties of Polymers*, 3rd. ed.; Wiley: New York, 1980.
(26) Etchenique, R. A.; Calvo, E. J. *Electrochem. Commun.* **1999**, *1* (4), 167.
(27) Atkinson, G.; Baumgartner, E.; Fernandez-Prini, R. *J. Am. Chem. Soc.* **1971**, *93*, 6436.
(28) Yang, H.; Kwak, J. *J. Phys. Chem. B* **1998**, *102*, 1982.
(29) Blanch, D. N.; Saveant, J. M. *J. Am. Chem. Soc.* **1992**, *114*, 3323.
(30) Bu, H.; English, A. M.; Mikkelsen, S. R. *J. Phys. Chem. B* **1998**, *101*, 9593.